Med-X (2024) 2:4
https://doi.org/10.1007/s44258-024-00018-2

Med-X

RESEARCH ARTICLE

Shear wave ultrasound elastography for estimating cartilage stiffness: implications for early detection of osteoarthritis

Elias Georgas[1] · Adnan Rayes[2] · Junhang Zhang[2] · Qifa Zhou[2,3] · Yi-Xian Qin[1]

Received: 29 December 2023 / Revised: 27 February 2024 / Accepted: 28 February 2024

Abstract

Current osteoarthritis (OA) diagnosis relies on radiographic abnormalities found in later stages of the disease, posing a challenge to the treatment efficacy. Therefore, earlier detection of OA is essential for improving therapeutic outcomes. The aim of this study was to investigate the feasibility of shear wave ultrasound elastography (SWUE) to detect changes in cartilage mechanical properties under OA conditions ex-vivo. Bovine osteochondral units were harvested from femoral condyles and subjected to either trypsin degradation, cartilage surface roughness defect using varying degrees of sandpaper, or subchondral bone degeneration using formic acid (FA) injection. Shear waves were generated using a mechanical shaker, while a high-frequency ultrasound system operating at 18 MHz was employed to detect wave propagation along the samples. The elasticity of cartilage was estimated by the shear wave speed (SWS) through the auto-correlation method. Our results show that the estimated SWS of cartilage after 24, 48, and 72 hours of trypsin incubation significantly decreased by 37%, 43%, and 59%, respectively, compared to the control group. Surface roughness treatment using 150-grit sandpaper significantly decreased the SWS by 35% compared to the control. Samples treated with 7% FA showed a significant increase in SWS by 62%, 89%, and 53% compared to control, 1% FA, and 3% FA, respectively. Our findings demonstrate the feasibility of SWUE to differentiate the elastic properties of cartilage under different OA conditions. This study presents the potential of a noninvasive, nonionizing tool for early detection of OA, representing a significant step toward its clinical implementation.

Elias Georgas and Adnan Rayes contributed equally to this work.

✉ Yi-Xian Qin
yi-xian.qin@stonybrook.edu

[1] Department of Biomedical Engineering, Stony Brook University, Stony Brook, NY 11794, USA

[2] Alfred E. Mann Department of Biomedical Engineering, University of Southern California, Los Angeles, CA, USA

[3] Department of Ophthalmology, University of Southern California, Los Angeles, CA, USA

Published online: 12 April 2024

Graphical Abstract

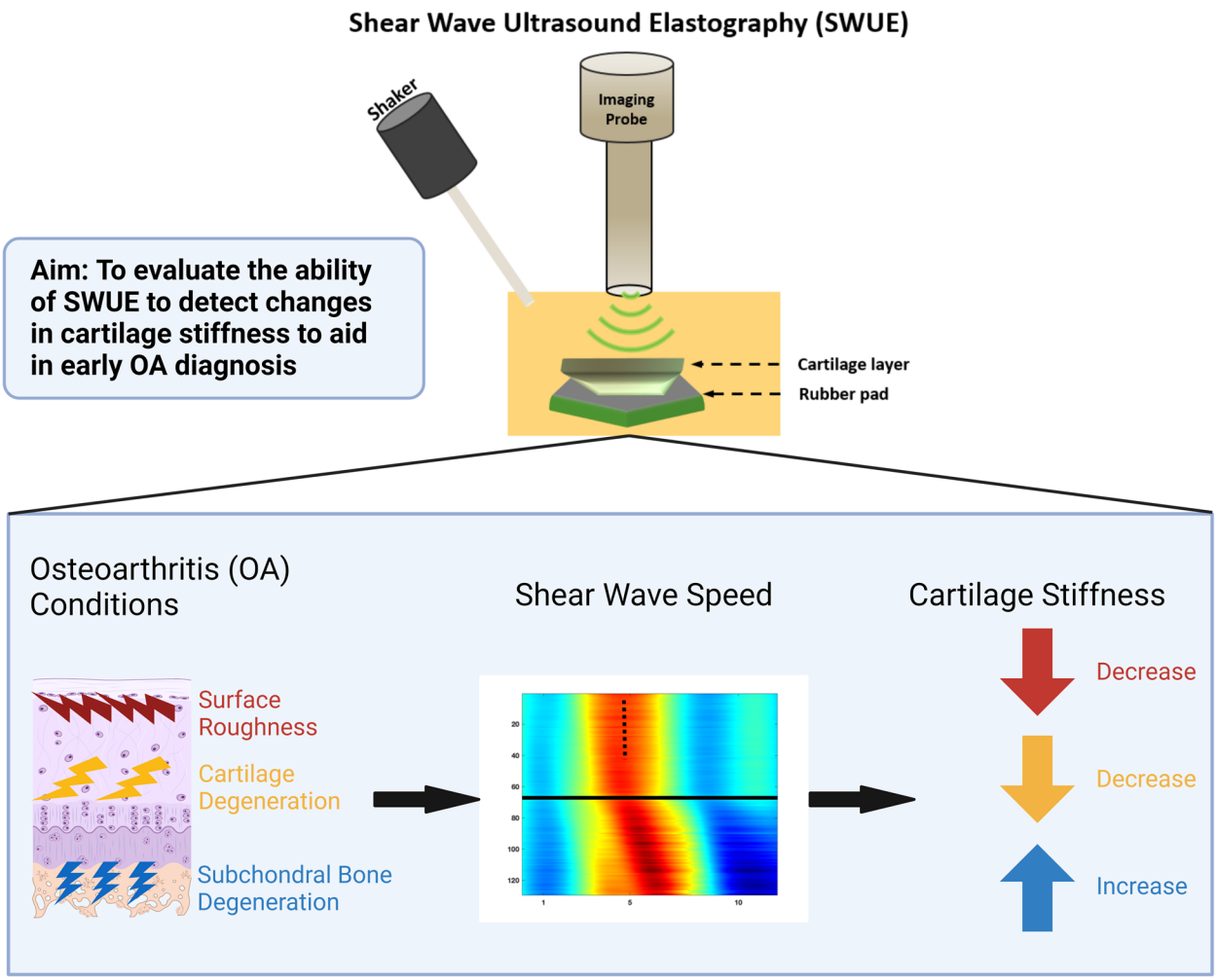

Highlights

- Shear wave ultrasound elastography noninvasively measure the elastic properties of soft tissue.
- Increasing cartilage surface roughness and enzyme degradation results in slower shear wave speeds.
- Subchondral bone degradation increases shear wave speed in cartilage.
- Shear wave ultrasound elastography is a novel method for early osteoarthritis diagnosis.

Keywords Osteoarthritis · Cartilage · Shear wave elastography · Shear wave speed · Ultrasound

Introduction

Osteoarthritis (OA) is a chronic degenerative joint disorder that is the leading cause of disability in the elderly population, affecting over 27 million Americans [1]. Primary symptoms of OA include joint pain, stiffness, and locomotor restriction. In addition, radiographic features such as osteophytes and joint space narrowing indicate cartilage loss, but these features do not always correlate with pain or functional impairment [2, 3]. Radiography also has poor soft tissue contrast, making early cartilage damage diagnosis challenging. Alternatively, magnetic resonance imaging (MRI) provides excellent soft tissue contrast and high spatial resolution, but the sensitivity is less than that of clinical and radiographic techniques in diagnosing OA [4]. Computed tomography is a more accurate modality to detect cortical

bony features, and is valuable in cases where MRI is contraindicated, but the risk of ionizing radiation exposure limits its use in OA diagnosis [5]. The visible morphological changes in OA diagnosis occur late in disease progression, making treatment strategies ineffective in reversing cartilage degeneration. Therefore, there is a clear need for early detection of cartilage degeneration to enhance treatment strategies.

In the early stages of OA, bone remodeling and subchondral bone loss are elevated. This is the initial step in abnormal mechanical loading by altering the joint shape and transmission [6]. The increased turnover leads to thinning and higher porosity of the subchondral bone plate that initiates progressive cartilage compositional changes [7], such as loss of proteoglycan content [8], loss of collagen content and organization [9], and changes in tissue hydration [10]. These deviations in subchondral bone and cartilage composition alter the mechanical properties of the tissue and mechanical function, which may contribute to further degeneration [11, 12]. Since these mechanical changes occur prior to the radiographic features, detection of these changes may prove to be a novel method in early OA diagnosis.

Shear Wave Ultrasound Elastography (SWUE) is a noninvasive imaging technique designed to assess the biomechanical properties of soft tissues. In order to provide valuable information about tissue stiffness, the technique employs a high frame rate (typically exceeding 500 frames/second) to capture the propagation of shear waves along the tissue [13, 14]. The research of this technique began in the late 1990s, and since then, the technique has been applied across various medical disciplines such as cardiac [13], Eye [15, 16], thrombus [17–19], Brain [20], Skin [21], and lung [22] tissues.

Recently, limited research has investigated the use of SWUE to study the mechanical properties of cartilage. In this context, our study builds upon existing efforts to advance the understanding of ultrasound elastography's role in detecting the mechanical properties of cartilage. Ginat et al. investigated the potential of high-resolution ultrasound elastography for assessing the mechanical properties of bovine articular cartilage. The study revealed near-zero strains within samples, except at specific locations like the articular surface and the interface between zones 1 and 2 during instantaneous static compression [23]. Despite successfully demonstrating strain imaging during compression, the study acknowledges challenges related to complex boundary conditions. Chung et al. used ultrasound elastography to assess depth-dependent mechanical properties in tissue-engineered cartilage. The study demonstrated the feasibility of validating elastography-predicted strains against finite-element analysis. They found that internal regions of engineered cartilage exhibited significantly higher local strain than the surface, highlighting the potential of ultrasound elastography for evaluating the mechanical properties of engineered cartilage [24]. Lee et al. developed a high-frequency ultrasound elastography system with a motorized rotation stage to address challenges in assessing the mechanical property, ex-vivo, in anisotropic, high-stiffness tissues such as cartilage and swine heart [25]. The presented results showed the system's capability to accurately evaluate the mechanical properties of high-stiffness tissues.

Most of these studies utilized SWUE based on both group and phase velocity methods to extract valuable information regarding the elasticity of cartilage. Other groups have developed the Lamb Wave model (LWM), which utilizes guided waves through thin layers to extract the viscoelastic properties of the materials. Xu et al. investigated the LWM to assess the viscoelastic properties of ex-vivo bovine tibial plateau cartilage. This work established a suitable measurement range and loading frequency through theoretical and numerical analyses. The study validated the effectiveness of LWM in measuring cartilage viscoelasticity, marking a crucial step toward the ultimate goal of in vivo applications [26]. In addition, Xu et al. established a shear wave propagation model using the LWM to study the cartilage-bone structure. The study highlights the capability to distinguish between bone and cartilage regions through wave speed measurements and offers a theoretical basis for utilizing shear wave methods to measure cartilage elasticity in vivo, potentially advancing the diagnosis of OA [27].

The primary objective of this study was to further assess the ability of SWUE to detect changes in cartilage stiffness using enzymatic or mechanical surface degeneration methods, while also investigating the impact of subchondral bone abnormalities on cartilage stiffness, ex-vivo, as well as confirming changes in cartilage structure using scanning electron microscopy (SEM). To achieve this goal, the study initially focused on assessing the system's ability to accurately detect shear wave speed (SWS) variations in thin layers, using phantoms with different thicknesses. Subsequently, the system was applied to conduct cartilage measurements, providing valuable insights for advancing early OA.

Methods and materials

Cartilage sample preparation

Bovine femurs were purchased from a local market approved by the United States Department of Agriculture, eliminating the need for Institutional Animal Care and Use Committee (IACUC) approval. Medial and lateral femoral

condyles were exposed, and visually healthy osteochondral units were cut into approximately 8 x 8mm sections. Excess debris was removed by washing in double distilled water, and the osteochondral units were stored at -20 °C until testing.

Simulated osteoarthritis conditions

Degeneration of the articular cartilage was achieved by utilizing the chemical action of the trypsin enzyme. Trypsin has been shown to digest proteoglycans with a slight effect on the collagen network, which can mimic cartilage degeneration in OA [28]. Osteochondral units were immersed into a 0.05% trypsin-ethylenediaminetetra-acetic acid solution (Gibco, Grand Island, NY) at 37°C for either 24, 48, or 72 hours (n=3/group). Control samples were immersed in Dulbecco's Modified Eagle Medium (Gibco, Grand Island, NY) for the same time periods. After trypsin incubation, samples were washed three times with phosphate buffered saline before testing. Previous studies have shown that cartilage surface roughness increases as the Osteoarthritis Research Society International (OARSI) grade increases [29]. To simulate this effect, cartilage surfaces were exposed to varying degrees of sandpaper grit, in which grits 320, 220, and 150 corresponded to OARSI grades 1, 2, and 3, respectively. The cartilage surface was passed over a 25 cm^2 sandpaper square (3M, St. Paul, MN) from medial to lateral and posterior to anterior directions 5 times to generate surface defects (n=4/group). Representative optical images of cartilage samples following surface roughness treatment are shown in Fig. 1 (Stemi SV 11 Apo, Carl Zeiss Inc., Jenna Germany). To test the effect of increasing subchondral bone porosity on cartilage, 0.2 ml of formic acid (FA), at concentrations of 1%, 3%, or 7% (Sigma Aldrich, St. Louis, MO) was injected into the subchondral bone using a 25g needle (n=3/group). The morphology of the cartilage surfaces was imaged with SEM (LEO1550, LEO, Germany) at 2.5 kV acceleration voltage and 4-7 mm working distance. Prior to imaging, the cartilage was carefully removed from subchondral bone, fixed in 4% paraformaldehyde for 24 hours, dehydrated by serial increasing ethanol concentrations, and dried in a desiccator. All cartilage samples were then sputter-coated with gold to improve surface conductivity.

Ultrasound: system setup and data processing

To evaluate tissue elasticity using shear wave ultrasound elastography, three main steps are involved: (1) Tissue deformation, (2) Image acquisition: capturing the tissue's deformation, and (3) Image reconstruction and analysis: correlate deformation to elasticity. Figure 2 shows a schematic diagram of the experimental setup, which is similar to [16, 17] except for the test sample and system parameters.

Tissue deformation

A mechanical shaker (#4810, Bruel & Kjaer, Duluth, Georgia, USA) connected to a metal rod (tip dimensions: 1.5 x 1 mm^2) that gently touched the surface of the sample was used to induce tissue deformation. The shaker was derived by a single pulse of 2 kHz sine wave, 500 mV through a function generator (AFG 3252C, Tektronix Inc., Beaverton, OR, USA) and amplified by a power amplifier (#2718, Bruel & Kjaer Co., Duluth, Georgia, USA).

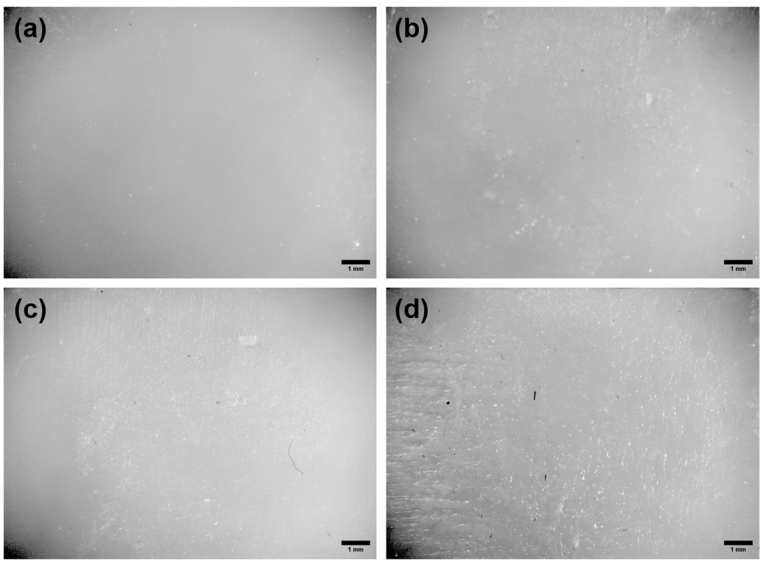

Fig. 1 Representative optical microscopy cartilage images following various surface roughness defects: (**a**) control, (**b**) 320 grit, (**c**) 220 grit, (**d**) 150 grit. Scale Bar: 1 mm

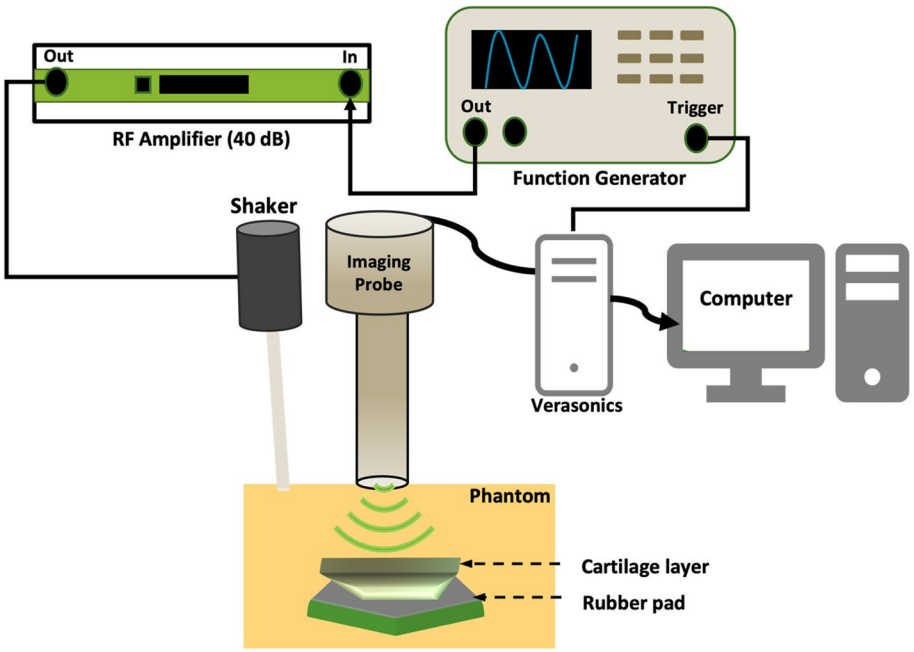

Fig. 2 Schematic diagram of shear wave elastography ex-vivo setup

Image acquisition

A programmable ultrasound research system (Vantage 256, Verasonics, Redmond, WA, USA) with an 18 MHz center frequency, 128 elements array probe (L22-14v, Verasonics, Redmond, WA, USA), placed laterally above the sample was used to detect the lateral shear waves propagation. Given the high stiffness nature of cartilage tissue, which could potentially result in high SWS ($C_s > 20$ m/s), a high frame rate should be considered [30]. Therefore, a frame rate of 10 kHz with three compounded angles was implemented in this study. The in-phase/quadrature (IQ) dataset, comprising 250 frames (equivalent to 25 ms of data acquisition), was collected and saved for offline post-processing. The probe was securely mounted on a five-axis stage to enable precise handling. Both the mechanical shaker and scanning probe were triggered by the ultrasound system and synchronized by the function generator. System parameters were maintained the same for both phantom and cartilage studies to eliminate bias.

Image reconstruction

B-mode images were utilized as a guide prior to the elastography experiment to accurately identify the location of the cartilage within the phantom and investigate its structural attributes, including thickness (Fig. 3h). The IQ data (total of 25 ms) obtained through B-mode images were processed through MATLAB (2021a, The MathWorks, Natick, MA, USA). As lateral shear waves propagate through successive data points (displacement of each imaging pixel), examining the similarity of these data points can provide information about the wave's behavior, including its speed. Hence, 1-D autocorrelation (Kasai algorithm) was implemented to calculate the dynamic displacement at each imaging pixel, providing insight into tissue displacement. Next, 2-D spatiotemporal maps were generated with lateral distance (representing the axial displacement) over time , with different colors indicating variations in displacement magnitude. The SWS based on group velocity method was estimated by applying linear regression to the lateral positions on the axial displacement map and their corresponding times (defined as the time to reach the peak displacement at each dynamic displacement) [21]. A bandpass filter was implemented to eliminate noise. The data processing and SWS estimation were rooted in prior research conducted by our group, except for the system parameters and some procedures due to cartilage behavior and geometry. This previous work involved the estimation of tissue elasticity in various tissues, including thrombus [17], posterior eye [31], optic nerve, sclera [15], and ciliary body [32]. Prior to the experiment, the samples were immersed in saline solution and allowed to equilibrate at room temperature for at least 30 minutes. To mitigate the temperature-related impact on the gelatin phantom, all the experiments were done at room temperature.

During the experiment, the tip of the rod (connected with the shaker) was touching the phantom a few millimeters away from the cartilage location. In some cases, we varied the shaker-probe distance to account for size and surface variations in cartilage, ensuring optimal lateral alignment across all samples. The imaging probe was precisely positioned above the cartilage. Following validation through phantom study, it is important to note the distance between

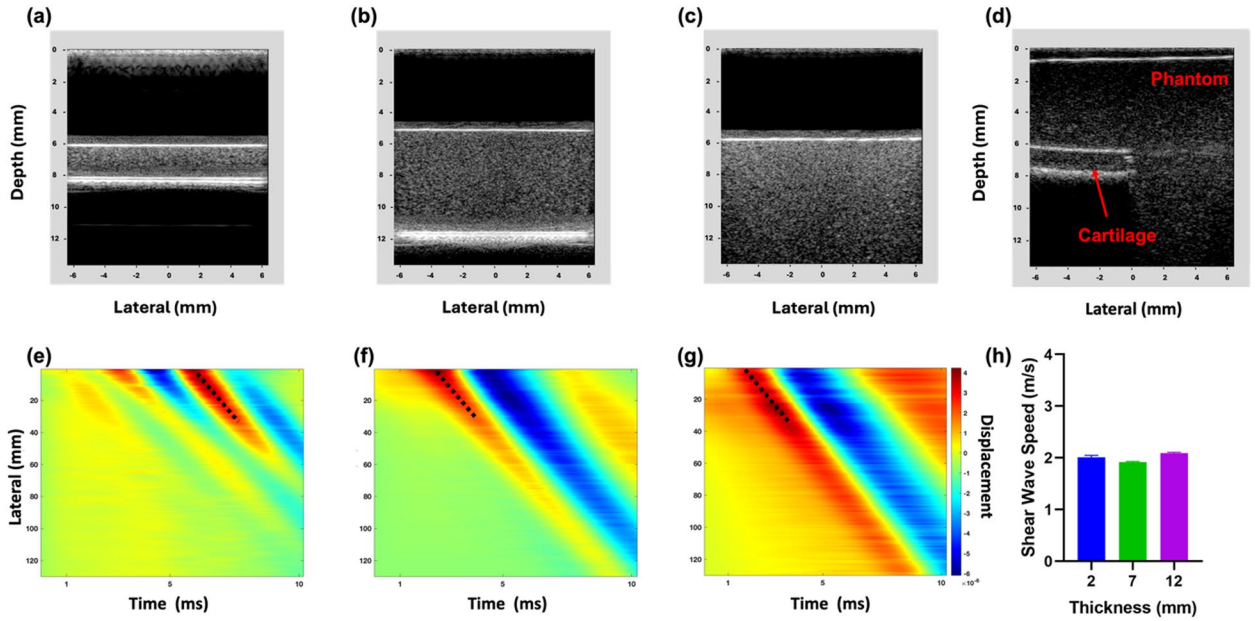

Fig. 3 Shear wave speed (SWS) is consistent across various phantom thicknesses. (**a**-**c**) B-mode images and (**e**-**g**) spatiotemporal maps of different thickness phantoms. (**a**, **e**) 2mm, (**b**, **f**) 7mm, and (**c**, **g**) 12 mm. The slope of the dotted line in (**e**-**g**) represents the estimated SWS. (**d**) Representative B-mode image of cartilage embedded in phantom. (**h**) Estimated SWS (mean ± SD) of 2, 7, and 12 mm thick phantoms were 2 ± 0.1 m/s (n=3)

the excitation and imaging probe may impact the propagation time of shear waves but had no significant effect on SWS measurement. In addition, our system setup is to assess the stiffness through shear waves that propagate laterally (along the probe). Positioning the shaker laterally along the imaging probe ensures the detection of the lateral propagation of shear waves along the sample. In addition, the lateral alignment maintains the integrity of shear waves over long distance [17, 21]. Therefore, the tip of the shaker was placed almost perpendicular to the imaging subject and along the imaging probe. Each sample's measurements were conducted three times; and the average value was calculated.

Phantom with different thickness

To validate the system parameters, tissue-mimicking gelatin phantoms with various thicknesses and the same stiffness were fabricated following the established protocol used by our group [15, 31]. In this work, homogeneous phantoms were fabricated using equal concentration of Gelatin (Gelatin G8-500, Fisher Scientific, USA) and silicon carbide powder (S5631, Sigma-Aldrich, St. Louis, MO, USA), resulting in phantoms with 2, 7, and 12 mm thickness (Fig. 3(a-c)). The primary objective of this part of the study was to ensure a consistent SWS across different phantom thicknesses (Fig. 3(h)).

Cartilage-embedded in phantom

Cartilage, being a layered, thin, and boundary-affected tissue, presents complexities that can affect the accuracy of elastography-based measurement. Boundary effects, such as reflections at the interface of cartilage and surrounding tissues, can distort the wave propagation behavior, leading to potentially inaccurate SWS estimation. Furthermore, low-thickness layers can make it difficult to distinguish true mechanical properties from those of adjacent tissues, and could lead to guided wave behavior [33]. Considering these challenges, this study adopts an innovative approach by embedding the cartilage into a gelatin phantom (Fig. 3(d)). This approach mitigates some of the challenges associated with cartilage samples, such as boundary and thin layer effects. Additionally, it aids in advancing this technology toward clinical practice, as the phantom effectively mimics the surrounding cartilage structure.

The cartilage samples, with their trapezoidal shape and uneven subchondral base, presented challenges for secure placement on a plate. To address this, the samples were placed in a container with a rubber pad attached to the base to minimize acoustic reflections. Additionally, the base of each sample was filled with epoxy to ensure stability during the experiment. After the epoxy had cured, the container was filled with gelatin phantom to encase the cartilage sample. Subsequently, the container was

transferred to 4°C for three hours. By embedding cartilage within the phantom, shear waves can propagate on a larger surface, thus reducing the impact of reflections. Additionally, positioning the shaker directly on the phantom and measuring the SWS at the cartilage location allows enough time for the waves to propagate and, thus, a more controlled and accurate assessment of cartilage mechanics.

Relating SWS with elasticity

Elastography-based technique is commonly quantified by estimating the group velocity and its association with the elastic modulus. With the cartilage-embedded phantom method, we opted to work with a bulk medium. Despite cartilage having distinct layers that may exhibit different mechanical properties, for the purposes of this study, we assumed uniform stiffness across all cartilage layers. Consequently, the average group velocity was calculated across the entire depth of the sample. The relation between elastic modulus and the SWS is given by [34]:

$$C_s = \sqrt{\frac{\mu}{\rho}} \tag{1}$$

Where C_s is the shear wave speed, μ is the elastic modulus, ρ is the tissue density. Based on this relation, higher SWS will indicate a stiffer sample, while lower SWS indicates a softer sample. Viscosity was ignored in this study, and only elastic property was considered.

Statistical analysis

All results were analyzed based on at least three independent experiments and expressed using standard deviation. Trypsin degradation results were analyzed by two-way ANOVA with Šídák's multiple comparisons test. Surface roughness and formic acid results were analyzed by one-way analysis of variance (ANOVA) with the Tukey post hoc test. *P* value less than 0.05 was considered to be a significant difference (GraphPad Prism version 9.3.0, San Diego, CA).

Results

In this work, we hypothesized that SWUE can detect changes in cartilage mechanical properties using simulated OA conditions. To test this hypothesis, and after validating the system capabilities of estimating SWS through phantom study, we first tested how enzymatic degradation of articular cartilage affects the SWS propagation along the cartilage layer. We then investigated the impact of surface defects of varying degrees on the SWS and whether differences can be detected. Finally, the effect of subchondral bone defects on cartilage surface SWS propagation was investigated.

Phantom thickness calibration

To ensure consistency in the estimated SWS across samples with varying thicknesses, phantoms with 2, 7, and 12 mm thicknesses were generated (Fig. 3(a-c)). The spatiotemporal maps showed similar slopes across each phantom thickness tested (Fig. 3(e-g)), and further quantification resulted in a consistent SWS of 2 ± 0.1 m/s for all phantoms (Fig. 3(h)). These results indicate the system's ability to estimate SWS accurately across different thickness layers.

Cartilage morphology

To confirm the alterations to the cartilage surface morphology using the simulated OA conditions, SEM imaging was conducted. After 24 hours of incubation in trypsin, the proteoglycans started to break down and small holes started forming in the extracellular matrix (ECM) compared to the control (Fig. 4(a, b)). The degradation started to continue after 48 and 72 hours of trypsin digestion (Fig. 4(d,f), where the control did not have any obvious alterations compared to 24 hours (Fig. 4(c,e). Surface roughness defect initiation using decreasing grits of sandpaper created pronounced defects in the cartilage surface with 150 grit inducing the greatest destruction (Fig. 5(d)). Compared to the control, 320 grit and 220 grit resulted in increased surface roughness, but were not significantly different from each other (Fig. 5(a-c)). After injection of increasing concentrations of FA into the subchondral bone, the cartilage surface became less porous and smoother than the control, with 7% FA having the greatest effect (Fig. 6(d)). Therefore, the simulated OA conditions used were able to initiate changes in the cartilage surface for detection using SWUE.

Cartilage degradation reduces SWS

To demonstrate if enzymatic cartilage degradation can affect SWS propagation, bovine osteochondral units were immersed in a trypsin-EDTA solution for 24, 48, and 72 hours, and the SWS was estimated using SWUE-based group velocity method. The spatiotemporal maps, with the vertical black dotted line, represent the estimated SWS that propagates along the lateral direction of the articular cartilage (Fig. 7). The control samples had consistent slopes in the spatiotemporal maps after 24, 48, and 72, hrs (Fig. 7(a-c)), while the samples with trypsin treatment slightly decreased the slopes, seen in the spatiotemporal maps at each time point (Fig. 7(d-f)). Further quantification of the estimated SWS showed that trypsin significantly reduced the SWS

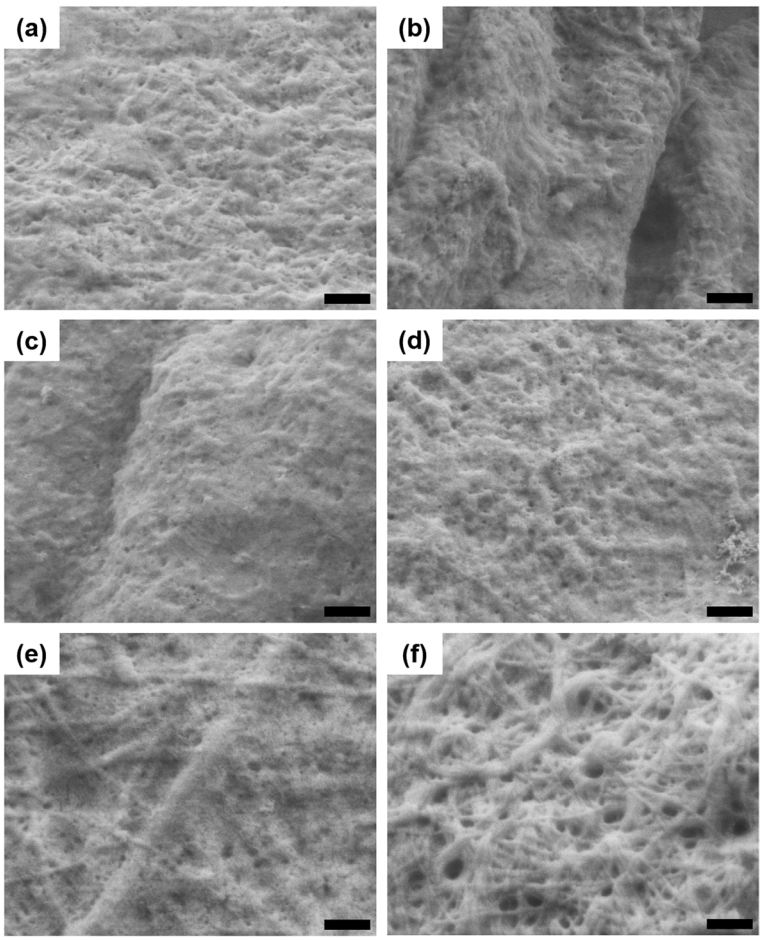

Fig. 4 Representative SEM images of cartilage surfaces following 24 hr, 48 hr, and 72 hr of control (**a**, **c**, **e**) or trypsin treatment (**b**, **d**, **f**). Scale bar: 500 nm

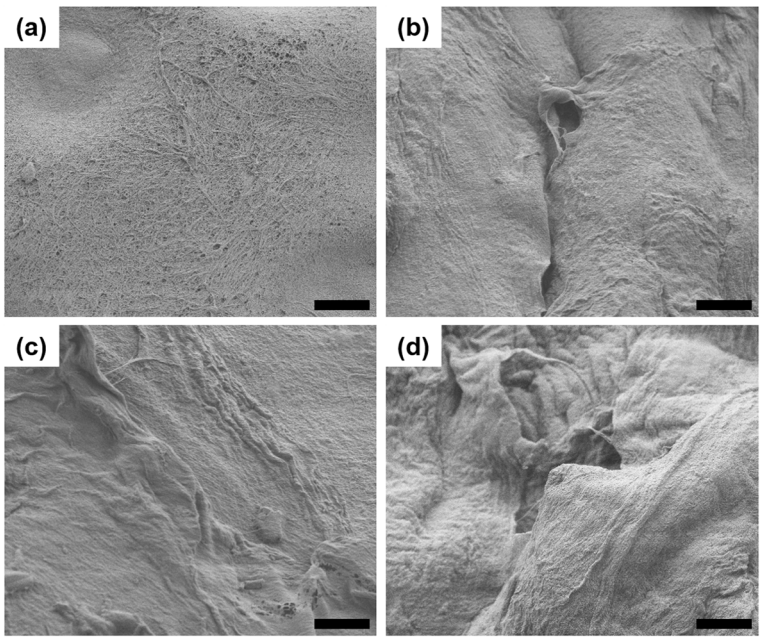

Fig. 5 Representative SEM images of cartilage surfaces of (**a**) control, (**b**) 320 grit, (**c**) 220 grit, (**d**) 150 grit treated samples. Scale bar: 10 µm

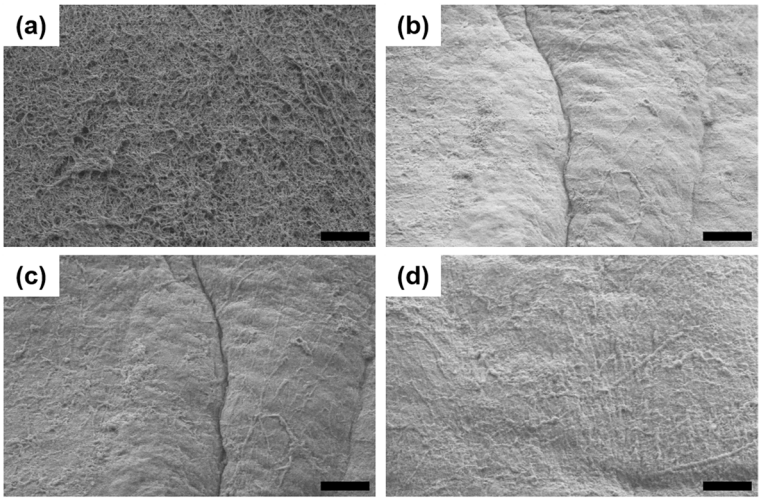

Fig. 6 Representative SEM images of cartilage surfaces of (**a**) control, (**b**) 1% formic acid, (**c**) 3% formic acid, and (**d**) 7% formic acid injections. Scale bar: 3 μm

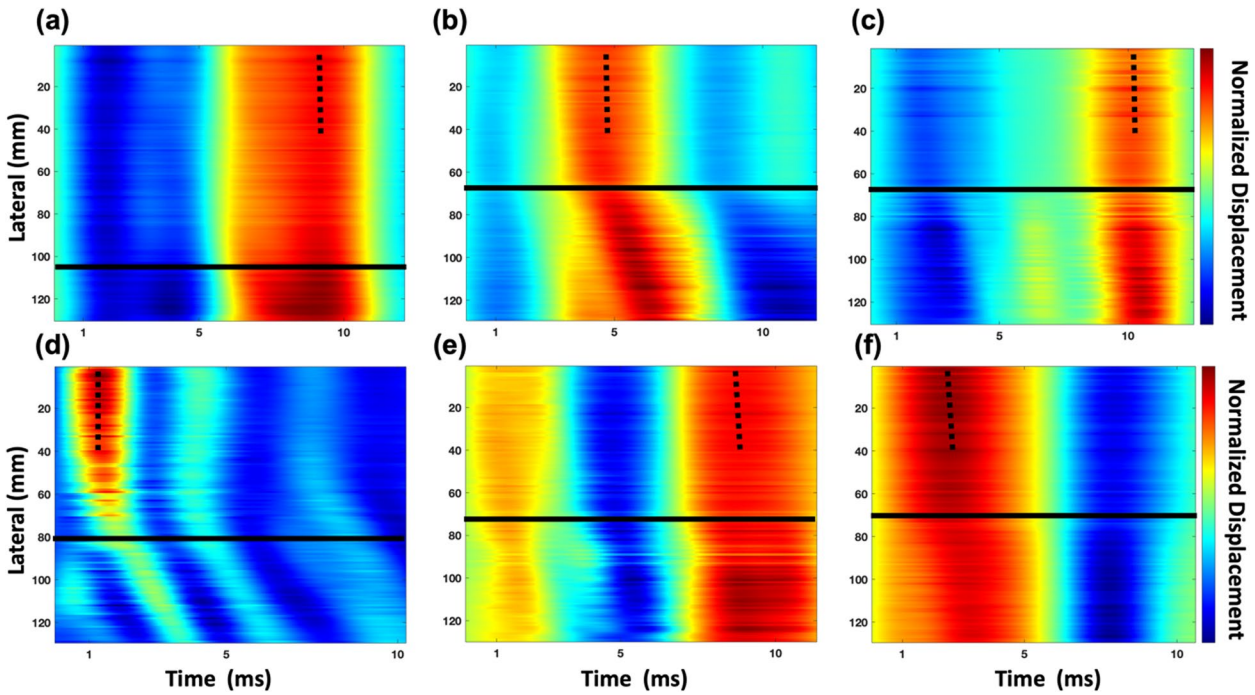

Fig. 7 Spatiotemporal maps of control (**a**-**c**) and trypsin treated (**d**-**f**) with different treatment durations: (**a**, **d**) 24 hrs, (**b**, **e**) 48 hrs, and (**c**, **f**) 72 hrs. The solid line delimits the boundary between the cartilage (above the line) and the phantom (below the line). The slope of the dotted line in represents the estimated SWS

compared to the control at 24, 48, and 72 hrs ($p<0.05$, $p<0.01$, and $p<0.001$, respectively) (Fig. 8(a)). In addition, there was a slight decrease in SWS from 24 to 48 hours of trypsin treatment (-8.7%) and further decreased from 48 to 72 hours (-18.3%), but the difference was not significant. Since higher SWS indicates stiffer cartilage, trypsin treatment reduced the SWS, indicating SWUE was able to detect the cartilage degradation.

Cartilage surface defect reduces SWS

Articular cartilage was mechanically degraded using varying degrees of sandpaper roughness to induce surface defects, and the SWS was estimated. The SWS significantly decreased after exposure to 150 grit compared to control, 320 grit, and 220 grit ($p<0.001$, $p<0.01$, $p<0.05$, respectively) (Fig. 8(b)). However, there was no significant

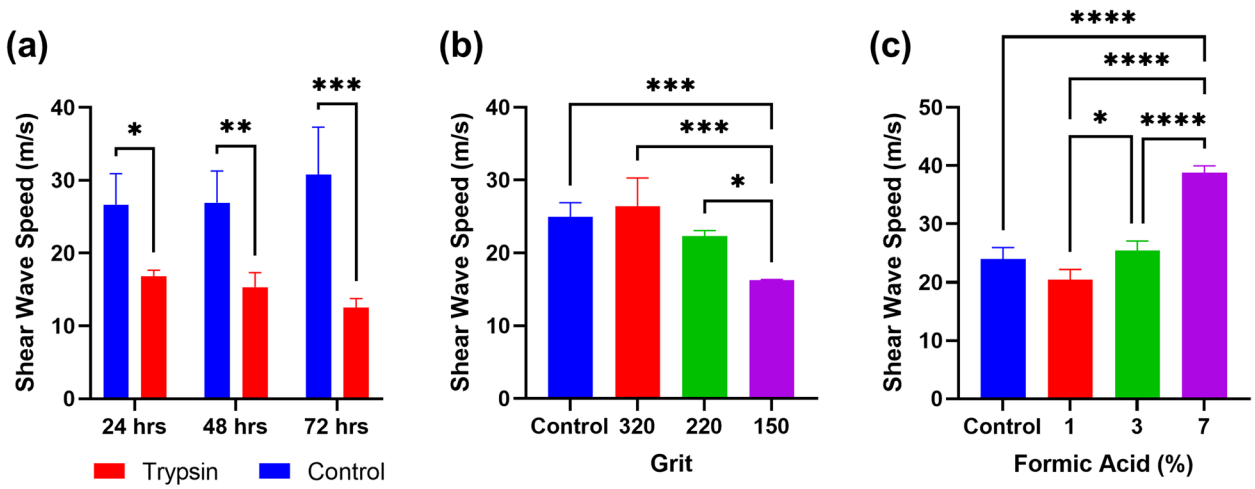

Fig. 8 Changes in cartilage SWS detected using SWUE after (**a**) trypsin degradation, (**b**) surface roughness defect, and (**c**) FA injection in subchondral bone. (*p<0.05, **p<0.01, ***p<0.001, ****p<0.0001)

difference in the control SWS compared to 320 grit and 220 grit (Fig. 8(b)), which is in agreement with the degree of surface abnormalities shown in Fig. 1 (a-c). These results suggest that SWUE can detect severe cartilage surface defects.

Subchondral bone degradation increases SWS

Subchondral bone degradation was initiated by adding different concentrations of FA (1, 5, and 7%), and SWS of the articular cartilage was measured to investigate the effect of subchondral bone on the cartilage elastic property. The SWS significantly increased after 7% FA injection by 62%, 89%, and 53% compared to control, 1% FA, and 3% FA, respectively (p<0.0001) (Fig. 8(c)). Furthermore, 3% FA injection resulted in a significantly greater SWS compared to 1% FA (p<0.05), but this increase was not significantly different from the control (Fig. 8(c)). The increase in SWS shows an increase in cartilage stiffness as increasing concentrations of FA are injected into the subchondral bone.

Discussion

In this work, we demonstrate that SWUE has the ability to detect differences in cartilage mechanical properties under simulated OA conditions. As shown in Fig. 8(a), our results indicate that the SWS on cartilage decreases after trypsin treatment, which continues over a 72-hour period. The decrease in SWS is related to a decrease in cartilage stiffness, which is consistent with previous studies where mechanical indentation showed 4 hours of trypsin treatment reduced cartilage stiffness [28]. Proteoglycans are essential in articular cartilage to provide osmotic pressure by binding to water, which assists in resisting compressive loads [35]. Trypsin is known to digest proteoglycans and have a slight effect on the collagen network in cartilage, but does not affect the cartilage thickness significantly [36–38]. The SEM images show increased degradation in the cartilage ECM after 24 hours of trypsin treatment and progressed at 48 and 72 hours, which is demonstrated by the increased in amount of space between fibers (Fig. 4). In addition, cartilage stiffness has been shown to decrease after proteoglycan digestion [39]. Therefore, the reduction in SWS from trypsin treatment is due to a decrease in cartilage stiffness.

During the progression of OA, the proteoglycan and collagen network degrade and reduce the mechanical strength of articular cartilage. Furthermore, tissue mineralization of the cartilage occurs in end-stage OA and could act as stress concentrations to initiate cracks in the cartilage [40, 41]. In fact, previous work has shown that the surface roughness of intact articular cartilage in OA further increases in response to mechanical loading compared to healthy cartilage due to the presence of mineral deposits in the superficial region [42]. To simulate this effect, we mechanically degraded the surface of articular cartilage using varying degrees of sandpaper roughness. Visually, use of the 150 grit sandpaper resulted in the greatest surface defects compared to control, 320-, and 220-grit, while the use of 320- and 220-grit had minimal surface defects (Fig. 5). As a result, the SWS significantly decreased from 150 grit compared to 320, 220 grit, and control. At the same time, there were no significant differences between 320, 220 grit, and control (Fig. 8(b)). The decrease in SWS indicates a reduction in cartilage stiffness, which is in accordance with previous work demonstrating that increasing the grade of OA is highly correlated to decreasing cartilage elastic and shear storage modulus [43, 44]. It is important to note that the mechanical degradation led to a minor reduction in signal-to-noise ratio (SNR),

which could underestimate the SWS along the entire sample. In this work, the SWS measurement was only acquired at regions with reasonable SNR.

Subchondral bone remodeling plays an important role in OA progression, which is suggested to occur prior to the degradation of articular cartilage. In the femoral head, it showed that subchondral bone collagen had a 20-fold increase in turnover and a 25% decrease in mineralization, which results in narrower and weaker fibers that weaken the mechanical properties of subchondral bone [45]. In addition, the subchondral bone plate modulus and hardness have been shown to progressively decrease in an OA rat model [46]. FA, a well-known decalcifying agent, was used to simulate the decrease in mineralization occurring in subchondral bone during OA progression. Since this remodeling process occurs before cartilage degradation, we tested how this decrease in subchondral bone mineralization affected cartilage stiffness. Figure 8(c) shows that 7% FA injection significantly increased the SWS compared to the control, 1%, and 3% FA. Interestingly, 3% formic acid significantly increased the SWS compared to 1%, but neither was significantly different from the control. The SEM images of the cartilage surfaces showed that the cartilage surface became less porous as the concentration of FA increased compared to the control, which may explain the increase in SWS (Fig. 6). Previous results have shown that there was a significant negative correlation between cartilage shear storage modulus and subchondral bone elastic modulus in OA [43], which is in agreement with these results. In addition, SWS was increased in the medial and intercondylar cartilage in patients with knee osteoarthritis in a preliminary clinical study [47]. Therefore, the increase in SWS may be an early predictor in OA, but requires further clinical evaluation.

Using ultrasound elastography, we were able to detect changes in cartilage mechanical properties under simulated OA conditions. However, only significant differences were found when cartilage was damaged to greater extents using 150 grit and 7% FA injections. For optimal system performance and stability, it was recommended to use a maximum of 10 kHz pulse repetition frequency. However, to accurately detect small changes in such hard tissue, a better sensitivity might be considered in the future to enhance the system's performance. In the data acquisition, a total of 25 ms of IQ data was gathered. However, due to the rapid shear wave propagation resulting in a swift measurement process, only the initial 10 ms of the acquired data was utilized and processed. In addition, as the shaker was consistently positioned at the phantom, variation of the maximum displacement occurrence time was observed in the spatiotemporal maps (Fig. 4) across different samples. This inconsistency may be attributed to the shaker's distance variation relative to imaging probe during each test. Although the SWS measurement may not significantly be affected by these variation (as discussed in method section), future enhancement in the experimental setup is recommended to enhance the uniformity and reliability of SWS measurements across all samples.

By embedding the cartilage within the phantom, we successfully mitigated the boundary effect and utilized the group velocity method for SWS estimation. This strategic approach not only addresses boundary conditions but also smooths the way for future advancements in transitioning from ex-vivo to in-vivo studies. Specifically, this innovative setup serves as a surrogate, mimicking the tissue environment between the cartilage and surrounding structures. It represents a notable development of the existing ex-vivo studies, marking a significant step toward clinical implementation.

The utilization of group velocity, while beneficial for SWS estimation, imposes limitations on our capacity to differentiate mechanical properties across distinct tissue layers. Previous research has demonstrated variations in mechanical properties among different cartilage layers, especially in the presence of OA [48]. Considering this, future investigations may benefit from extracting multiple frequency information to potentially enhance the accuracy of SWS estimation.

In this study, we proved that SWUE is a novel approach to detecting changes in the mechanical properties of cartilage after enzymatic degradation, surface roughness defect, and subchondral bone degeneration. Cartilage degradation and increased surface roughness decreased the SWS, while increased subchondral bone degeneration increased the SWS, which indicated changes in cartilage stiffness. The results demonstrated a promising noninvasive and nonionizing technique to aid in early OA diagnosis.

Acknowledgments The authors would like to acknowledge Carmen Shum for helping with the preparation of cartilage samples for SWUE analysis. The authors would also like to thank Dr. Hsiao Chuan Liu for his technical support in ultrasound elastography system. The authors would like to extend their gratitude to Dr. James Quinn with his assistance in SEM imaging. A. Rayes is supported by King Abdulaziz University postgraduate scholarship. Graphical abstract was created using Biorender.com.

Authors' contributions Conceptualization: YX Qin and Q Zhou; Methodology: E Georgas, A Rayes, and YX Qin; Formal analysis and investigation: E Georgas, A Rayes, and J Zhang; Writing-original draft preparation: E Georgas and A Rayes; Writing-review and editing: YX Qin and Q Zhou; Funding Acquisition: YX Qin and Q Zhou; Resources: YX Qin and Q Zhou; Supervision: YX Qin and Q Zhou.

Funding This work was partially supported by the NIH REACH program, and the National Space Biomedical Research Institute through NASA Cooperative Agreement NCC 9-58, and NASA.

Availability of data and materials The data presented in this study are available on request from the corresponding author.

Declarations

Ethics approval and consent to participate This study does not require ethics approval since samples from post-mortem animals were used.

Consent for publication All authors have read and agreed to the published version of the manuscript.

Competing interests The authors declare no conflict of interest.

References

1. Lawrence RC, et al. "Estimates of the prevalence of arthritis and other rheumatic conditions in the United States. Part II," (in eng). Arthritis Rheum. 2008;58(1):26–35.
2. Glyn-Jones S, et al. "Osteoarthritis," (in eng). Lancet. 2015;386(9991):376–87.
3. Hayashi D, Roemer FW, Guermazi A. "Imaging for osteoarthritis," (in eng). Ann Phys Rehabil Med. 2016;59(3):161–9.
4. Menashe L, et al. "The diagnostic performance of MRI in osteoarthritis: a systematic review and meta-analysis," (in eng). Osteoarthr Cartil. 2012;20(1):13–21.
5. Sakellariou G, et al. EULAR recommendations for the use of imaging in the clinical management of peripheral joint osteoarthritis. Ann Rheum Dis. 2017;76(9):1484–94.
6. Castañeda S, Roman-Blas JA, Largo R, Herrero-Beaumont G. Subchondral bone as a key target for osteoarthritis treatment. Biochem Pharmacol. 2012;83(3):315–23.
7. Intema F, et al. "In early OA, thinning of the subchondral plate is directly related to cartilage damage: results from a canine ACLT-meniscectomy model," (in eng). Osteoarthr Cartil. 2010;18(5):691–8.
8. Thompson RC Jr, Oegema TR Jr. "Metabolic activity of articular cartilage in osteoarthritis. An in vitro study," (in eng). J Bone Joint Surg Am. 1979;61(3):407–16.
9. Hollander AP, Pidoux I, Reiner A, Rorabeck C, Bourne R, Poole AR. "Damage to type II collagen in aging and osteoarthritis starts at the articular surface, originates around chondrocytes, and extends into the cartilage with progressive degeneration," (in eng). J Clin Invest. 1995;96(6):2859–69.
10. Rivers PA, et al. "Osteoarthritic changes in the biochemical composition of thumb carpometacarpal joint cartilage and correlation with biomechanical properties," (in eng). J Hand Surg Am. 2000;25(5):889–98.
11. Guilak F. "Biomechanical factors in osteoarthritis," (in eng). Best Pract Res Clin Rheumatol. 2011;25(6):815–23.
12. Knecht S, Vanwanseele B, Stüssi E. "A review on the mechanical quality of articular cartilage - implications for the diagnosis of osteoarthritis," (in eng). Clin Biomech (Bristol, Avon). 2006;21(10):999–1012.
13. Caenen A, et al. Assessing cardiac stiffness using ultrasound shear wave elastography. Phys Med Biol. 2022;67(2):02TR01.
14. Gennisson JL, Deffieux T, Fink M, Tanter M. "Ultrasound elastography: principles and techniques," (in eng). Diagn Interv Imaging. 2013;94(5):487–95.
15. Qian X, et al. "Ultrasonic elastography to assess biomechanical properties of the optic nerve head and peripapillary sclera of the eye," (in eng). Ultrasonics. 2021;110:106263.
16. Weng CC, Chen PY, Chou D, Shih CC, Huang CC. "High Frequency Ultrasound Elastography for Estimating the Viscoelastic Properties of the Cornea Using Lamb Wave Model," (in eng). IEEE Trans Biomed Eng. 2021;68(9):2637–44.
17. Rayes A, et al. "Estimating thrombus elasticity by shear wave elastography to evaluate ultrasound thrombolysis for thrombus with different stiffness," (in eng). IEEE Trans Biomed Eng. 2023;70(1):135–43.
18. Xie H, et al. "Correspondence of ultrasound elasticity imaging to direct mechanical measurement in aging DVT in rats," (in eng). Ultrasound Med Biol. 2005;31(10):1351–9.
19. Liu HC, et al. "Characterizing blood clots using acoustic radiation force optical coherence elastography and ultrasound shear wave elastography," (in eng). Phys Med Biol. 2021;66(3):035013.
20. Lay FY, Chen PY, Cheng HF, Kuo YM, Huang CC. "Ex Vivo Evaluation of Mouse Brain Elasticity Using High-Frequency Ultrasound Elastography," (in eng). IEEE Trans Biomed Eng. 2019;66(12):3426–35.
21. Tsai WY, Hsueh YY, Chen PY, Hung KS, Huang CC. "High-Frequency Ultrasound Elastography for Assessing Elastic Properties of Skin and Scars," (in eng). IEEE Trans Ultrason Ferroelectr Freq Control. 2022;69(6):1871–80.
22. Zhou B, Yang X, Zhang X, Curran WJ, Liu T. "Ultrasound Elastography for Lung Disease Assessment," (in eng). IEEE Trans Ultrason Ferroelectr Freq Control. 2020;67(11):2249–57.
23. Ginat DT, Hung G, Gardner TR, Konofagou EE. High-resolution ultrasound elastography of articular cartilage in vitro. Intl Conf Proc IEEE Eng Med Biol Soc. 2006:6644–7. https://doi.org/10.1109/IEMBS.2006.260910.
24. Chung CY, Heebner J, Baskaran H, Welter JF, Mansour JM. "Ultrasound elastography for estimation of regional strain of multilayered hydrogels and tissue-engineered cartilage," (in eng). Ann Biomed Eng. 2015;43(12):2991–3003.
25. Lee S, Eun LY, Hwang JY, Eun Y. Ex vivo evaluation of mechanical anisotropic tissues with high-frequency ultrasound shear wave elastography. Sensors. 2022;22(3):978. https://doi.org/10.3390/s22030978.
26. Xu H, Shi L, Chen S, Zhang X, An KN, Luo ZP. "Viscoelasticity measurement of ex vivo bovine cartilage using Lamb wave method," (in eng). Phys Med Biol. 2018;63(23):235019.
27. Xu H, Chen S, An K-N, Luo Z-P. Near field effect on elasticity measurement for cartilage-bone structure using Lamb wave method. BioMed Eng OnLine. 2017;16(1):123.
28. Wang SZ, Huang YP, Saarakkala S, Zheng YP. "Quantitative assessment of articular cartilage with morphologic, acoustic and mechanical properties obtained using high-frequency ultrasound," (in eng). Ultrasound Med Biol. 2010;36(3):512–27.
29. Niu H-J, Wang Q, Wang Y-X, Li D-Y, Fan Y-B, Chen W-F. "Ultrasonic reflection coefficient and surface roughness index of OA articular cartilage: relation to pathological assessment. BMC Musculoskelet Disord. 2012;13(1):34.
30. Sarvazyan AP, Urban MW, Greenleaf JF. "Acoustic waves in medical imaging and diagnostics," (in eng). Ultrasound Med Biol. 2013;39(7):1133–46.
31. Qian X, et al. "In vivo evaluation of posterior eye elasticity using shaker-based optical coherence elastography," (in eng). Exp Biol Med (Maywood). 2020;245(4):282–8.

32. Zhang J, et al. “High-Frequency Ultrasound Elastography to Assess the Nonlinear Elastic Properties of the Cornea and Ciliary Body,” (in eng). IEEE Trans Ultrason Ferroelectr Freq Control. 2022;69(9):2621–9.
33. Shih CC, et al. Quantitative assessment of thin-layer tissue viscoelastic properties using ultrasonic micro-elastography with lamb wave model. IEEE Trans Med Imag. 2018;37(8):1887–98.
34. Nowicki A, Dobruch-Sobczak K. “Introduction to ultrasound elastography,” (in eng). J Ultrason. 2016;16(65):113–24.
35. Roughley PJ, Lee ER. “Cartilage proteoglycans: structure and potential functions,” (in eng). Microsc Res Tech. 1994;28(5):385–97.
36. Harris ED Jr, Parker HG, Radin EL, Krane SM. “Effects of proteolytic enzymes on structural and mechanical properties of cartilage,” (in eng). Arthritis Rheum. 1972;15(5):497–503.
37. Lu MH, Zheng YP, Huang QH. “A novel noncontact ultrasound indentation system for measurement of tissue material properties using water jet compression,” (in eng). Ultrasound Med Biol. 2005;31(6):817–26.
38. Lyyra T, et al. “Experimental validation of arthroscopic cartilage stiffness measurement using enzymatically degraded cartilage samples,” (in eng). Phys Med Biol. 1999;44(2):525–35.
39. Qin L, Zheng Y, Leung C, Mak A, Choy W, Chan K. “Ultrasound detection of trypsin-treated articular cartilage: its association with cartilaginous proteoglycans assessed by histological and biochemical methods,” (in eng). J Bone Miner Metab. 2002;20(5):281–7.
40. Fuerst M, Niggemeyer O, Lammers L, Schäfer F, Lohmann C, Rüther W. Articular cartilage mineralization in osteoarthritis of the hip. BMC Musculoskelet Disord. 2009;10:1–8.
41. Sadeghi H, Lawless BM, Espino D, Shepherd D. Effect of frequency on crack growth in articular cartilage. J Mech Behav Biomed Mater. 2018;77:40–6.
42. Cooke ME, Lawless BM, Jones SW, Grover LM. Matrix degradation in osteoarthritis primes the superficial region of cartilage for mechanical damage. Acta Biomaterialia. 2018;78:320–8.
43. Peters AE, Akhtar R, Comerford EJ, Bates KT. “The effect of ageing and osteoarthritis on the mechanical properties of cartilage and bone in the human knee joint,” (in eng). Sci Rep. 2018;8(1):5931.
44. Wilusz RE, Zauscher S, Guilak F. “Micromechanical mapping of early osteoarthritic changes in the pericellular matrix of human articular cartilage,” (in eng). Osteoarthr Cartil. 2013;21(12):1895–903.
45. Bailey AJ, Mansell JP, Sims TJ, Banse X. “Biochemical and mechanical properties of subchondral bone in osteoarthritis,” (in eng). Biorheology. 2004;41(3–4):349–58.
46. Yu DG, et al. “Dynamic Alterations in Microarchitecture, Mineralization and Mechanical Property of Subchondral Bone in Rat Medial Meniscal Tear Model of Osteoarthritis,” (in eng). Chin Med J (Engl). 2015;128(21):2879–86.
47. Yokuş A, Toprak M, Arslan H, Toprak N, Akdeniz H, Gündüz AM. Evaluation of distal femoral cartilage by B-mode ultrasonography and shear wave elastography in patients with knee osteoarthritis: a preliminary study. Acta Radiologica. 2021;62(4):510–4.
48. Niu H, et al. "Relationship between triphasic mechanical properties of articular cartilage and osteoarthritic grade. Sci China Life Sci. 2012;55(5):444–51.